This is an Accepted Manuscript version of the following article, accepted for publication in:

A. Arruti, J. Anzola, F. J. Pérez-Cebolla, I. Aizpuru and M. Mazuela, "The Composite Improved Generalized Steinmetz Equation (ciGSE): An Accurate Model Combining the Composite Waveform Hypothesis With Classical Approaches," in IEEE Transactions on Power Electronics, vol. 39, no. 1, pp. 1162-1173, Jan. 2024.

DOI: https://doi.org/10.1109/TPEL.2023.3323577

The Composite Improved Generalized Steinmetz Equation (ciGSE): an Accurate Model Combining the Composite Waveform Hypothesis with Classical Approaches

Asier Arruti[1], Jon Anzola[1], Francisco Jose Perez-Cebolla[2], Iosu Aizpuru[1], and Mikel Mazuela[1]

***Abstract*- Predicting core losses is a difficult task for designing magnetic components. Under triangular current waveforms, the classical approaches work with duty cycles close to 0.5, but are inaccurate for high and low duty cycles. In this work the composite waveform hypothesis is tested, using data from the MagNet database for N87 material at 25 ºC (3312 data points). Limitations of the composite waveform hypothesis are discussed, and a technique to expand the loss space is presented. The new approach based in an extended loss space is validated against the classical improved Generalized Steinmetz Equation, reducing the root mean square and 95 percentile errors by 5.85 and 6.96 times, allowing to predict core losses accurately even at high and low duty cycles. A direct correlation between the expanded loss space and the Steinmetz parameters from the improved Generalized Steinmetz Equation is proven, allowing to represent the core losses as functions of these parameters and generating the composite improved Generalized Steinmetz Equation. The proposed methodology for core loss prediction is validated making use of all data available from the MagNet database (10 materials, 4 temperatures, 59423 data points), achieving better results than the commonly used improved Generalized Steinmetz Equation.**

***Index Terms*- Core losses, Ferrites, Magnetic devices, MagNet challenge.**

I. INTRODUCTION

The design of magnetic components for higher frequency and power density applications is a challenging task. Not only the parasitic elements of the device must be taken into account, but also at these conditions, the reduced size of these devices makes thermal management difficult. An accurate prediction of power losses is necessary for an adequate design, but the complexity of the power losses, specially the core losses, makes it hard to achieve accurate loss predictions. Because of this, to avoid a prototyping and redesign process, it is common to tend to oversize the magnetic components to ensure the designs work properly.

The problem is more complex when considering the many parameters that influence core losses: flux density (B) and frequency (f), waveform, temperature, DC magnetization… Manufacturers typically only present data for sinusoidal waveforms and the power converters employed in high frequency high power density applications commonly operate with triangular or trapezoidal current waveforms, more common in switch mode power supplies. Because of this, other approaches are necessary to estimate the core losses.

A common approach to estimate core losses is to use experimental equations. The Steinmetz Equation (SE) (1), sometimes referred to as the power equation, is a well-known example, where the core losses per unit of volume (P_v) are related to the Steinmetz parameters (k, α, and β) [1]. This approach is based on sinusoidal excitation core loss data, so the Steinmetz parameters can be extracted from experimental data given in datasheets, but cannot be used to estimate core losses with non-sinusoidal waveforms.

$$P_v = k \cdot f^{\alpha} \cdot B^{\beta} \tag{1}$$

$$P_v = \frac{1}{T}\int_0^T k_i \cdot \left|\frac{dB}{dt}\right|^{\alpha} \cdot \Delta B^{\beta-\alpha} \tag{2}$$

$$k_i = \frac{k}{(2\pi)^{\alpha-1}\int_0^{2\pi}|\cos\theta|^{\alpha}|\sin\theta|^{\beta-\alpha}d\theta} \tag{3}$$

Numerous modifications of the SE have been proposed to predict the losses under non-sinusoidal excitation; most notably the Modified Steinmetz Equation (MSE) [2], the Generalized Steinmetz Equation (GSE) [3], and the improved Generalized Steinmetz Equation (iGSE) [4]. Due to its simplicity and satisfactory accuracy, the iGSE (2) with k_i defined by (3) is the

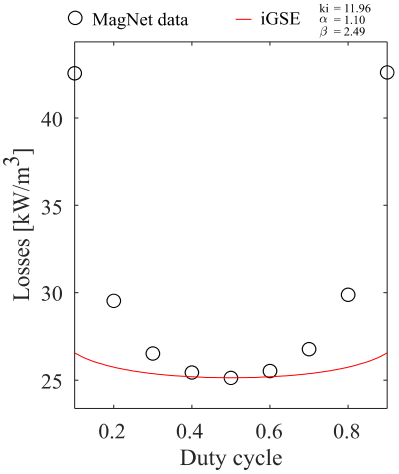

Fig. 1: Core loss prediction with iGSE for $D \in [0.1, 0.9]$. Experimental data from MagNet for material N87 at 25 ºC, f = 100 kHz and ΔB = 100 mT, with Steinmetz parameters extracted in the range of $f \pm 25$ % and $\Delta B \pm 25$ %.

The researchers acknowledge the financial support from the Department of Education of the Basque Government.

[1]Mondragon Unibertsitatea, Faculty of Engineering, Electronic and Computing Department

[2]University of Zaragoza, EINA, Department of Electronic Engineering and Communications

most common approach for core loss prediction for triangular and trapezoidal waveforms. However, the accuracy of the iGSE degrades significantly for triangular waveforms of low or high duty cycle (D), commonly when $D \notin [0.3, 0.7]$. This is visualized in Fig. 1, where the MagNet data of ferrite N87 at 25 ºC is used, and discrepancies > 50 % appear.

The focus on this work is to generate a model capable to simply yet accurately predict the core losses for different values of duty cycle. First, **Section II** presents a short review about existing methods to estimate core losses with variable duty cycles, pointing the key contributions and practical disadvantages of these methods. After concluding that the Composite Waveform Hypothesis (CWH) plays a key role in all these works, **Section III** analyses the fidelity of the CWH in a wide data range making use of the open-source MagNet core loss database for material N87 at 25ºC (3312 data points). Then, **Section IV** presents a novel approach to overcome the practical limitations of the CWH by introducing the concept of expanded loss spaces, allowing the accurate prediction of core losses in a 2.5 times wider data range. **Section V** mathematically proves a connection between these expanded loss spaces and the classical Steinmetz equation based approaches, thus the decision to name the presented method the composite improved Generalized Steinmetz Equation (ciGSE). Lastly, in **Section VI** the methodology is evaluated with other materials and temperatures from the MagNet database, using 59423 data points, proven the generalizability of the presented methodology.

Two appendixes are presented to illustrate the steps necessary to use the methodology. **APPENDIX A** clarifies how to extract the expanded loss spaces from experimental data, and defines the parameters used in this work. **APPENDIX B** demonstrates how the model can be implemented in a specific case of interest, and also demonstrates the capability to combine the model with other relevant publications.

II. Prediction Of Losses With Variable Duty Cycle

Several methods to better predict the core losses under non symmetrical triangular excitation these conditions have been proposed in the literature:

- In [5] a Double Natural Steinmetz Equation (DNSE) is presented, which is able to more accurately represent the tendency in power losses and achieves a better accuracy when $D \notin [0.3, 0.7]$.
- In [6] the Composite Waveform Hypothesis (CWH) is proposed, which assumes that the sum of the losses of each waveform segment equals the total losses of the waveform. Good predictions are achieved for triangular waveforms, although its dependency in experimental data from waveforms with $D = 0.5$ limits its application range.
- In [7] the concept of using individual Steinmetz parameters for each segment of the waveform is proposed. An analysis of the variability of the Steinmetz parameters is presented and the Improved Steinmetz Equation (ISE) is presented. Good accuracies are published for 100 kHz triangular waveforms when $D \in [0.05, 0.95]$.

Although the methodologies differ notably, all of these achieve a higher accuracy due to a better definition of the power losses in each segment. In fact, for a triangular waveform the ISE takes the form (4) that closely resembles the iGSE under the same condition (5). Excluding the use of variable Steinmetz parameters for each waveform segment, the major difference between these works is that the ISE uses the Flux Waveform Coefficient ($\pi/4 \cdot k_n$ for triangular waveforms) presented in [8] to approximate the losses for non-sinusoidal cases instead of the k_i parameter. The other differences are integrated in the k_i value for constant Steinmetz parameters. The summation terms indicates that the ISE makes similar assumptions as the CWH.

$$P_v = \sum_n \frac{\pi}{4} \cdot k_n D_n \left(\frac{f}{2D_n}\right)^{\alpha_n} B^{\beta_n} \tag{4}$$

$$P_v = \sum_n k_i \cdot D_n \left(\frac{f}{D_n}\right)^{\alpha} \Delta B^{\beta} \tag{5}$$

Overall, the available literature suggests that the assumption of the CWH is an effective approach to improve the accuracy when $D \notin [0.3, 0.7]$. Additionally, (4) and (5) suggest that the losses of each segment should be a function of an "effective frequency" and flux density.

III. Core Loss Space

The CWH [6] assumes any triangular waveform can be divided into two segments, so that the total core losses are obtained by combining the losses of each segment. Thus, for the asymmetrical waveform AB composed by the segments A and B (Fig. 2a), the equality (6) holds true. Since the segments A and B can also be used to form the symmetrical waveforms AA (Fig. 2b) and BB (Fig. 2c) where $D = 0.5$. The core losses P_{AA} and P_{BB} can then be extracted from symmetrical triangular

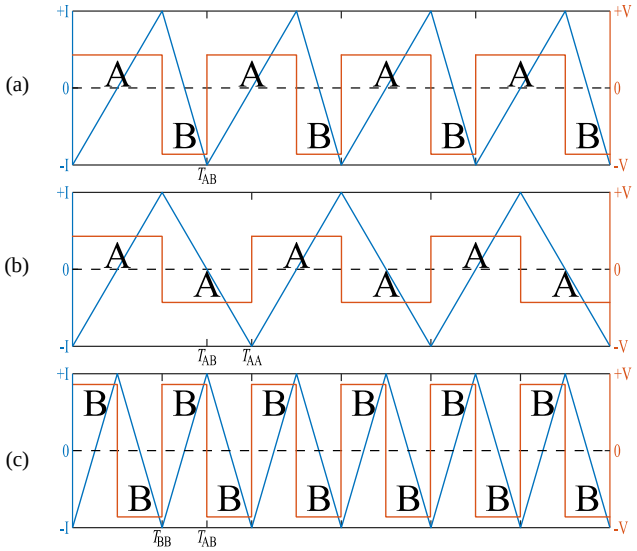

Fig. 2: Core loss decomposition of (a) waveform AB with D = 0.67 into (b) waveforms AA and (c) waveform BB according to the CWH [6].

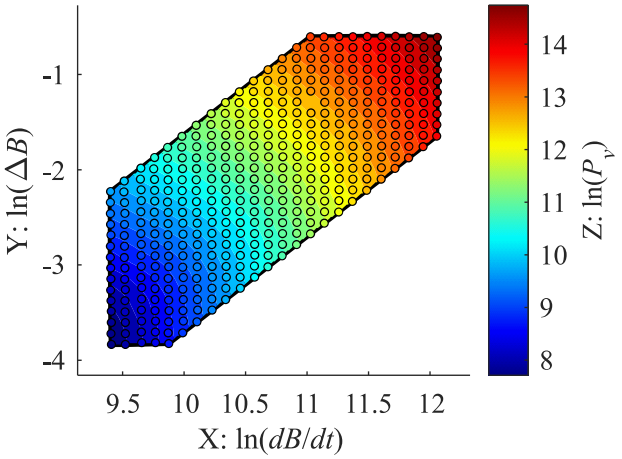

Fig. 3: Core loss space obtained from the MagNet data for material N87 at 25 ºC. The boundary of the loss space is highlighted in black.

waveforms of the equivalent frequencies $f_{AA} = f_{AB}/(2D)$ and $f_{BB} = f_{AB}/(2\text{-}2D)$ and flux density amplitudes $\Delta B_{AB} = \Delta B_{AA} = \Delta B_{BB}$.

$$P_{AB} = DP_{AA} + (1 - D)P_{BB} \tag{6}$$

The MagNet online database is used in this study due to the numerous experimental data available [9]-[12]. In this case, triangular waveform data for material N87 at 25 ºC without DC magnetization is analyzed. The data covers a wide frequency and flux density range: $f \in [55, 445]$ kHz and $\Delta B \in [20, 550]$ mT.

From the $D = 0.5$ data, the core loss space shown in Fig. 3 is constructed, since according to the assumption (6) $P_{AA} = P_{BB} = P_{AB}$. As expected, the maximum and minimum losses are obtained at high and low $|dB/dt|$ and ΔB, respectively. To make the loss space more manageable, the scattered data is fitted to a polynomial surface, where the XYZ dimensions are $\ln(|dB/dt|)$, $\ln(\Delta B)$ and $\ln(P_v)$, respectively. When defined as a polynomial surface of n degrees, the loss space takes the form (7). The necessary coefficients for the fitted fifth degree polynomial surface are shown in TABLE I.

TABLE I
COEFFICIENTS FOR FIFTH DEGREE FITTED LOSS SPACE

	p_{n0}	p_{n1}	p_{n2}	p_{n3}	p_{n4}	p_{n5}
p_{0n}	3626	3114	737.8	77.69	3.831	0.07067
p_{1n}	-1297	-945.7	-169.2	-11.87	-0.2922	0
p_{2n}	183.4	107.6	12.92	0.4532	0	0
p_{3n}	-12.7	-5.426	-0.3285	0	0	0
p_{4n}	0.4283	0.1024	0	0	0	0
p_{5n}	-5.547E-3	0	0	0	0	0

$$P_v = \exp\left(\left[\ln\left(\left|\frac{dB}{dt}\right|\right)^0 \quad \cdots \quad \ln\left(\left|\frac{dB}{dt}\right|\right)^n\right] \times \begin{bmatrix} p_{00} & \cdots & p_{0n} \\ \vdots & \ddots & \vdots \\ p_{n0} & \cdots & p_{nn} \end{bmatrix} \times \begin{bmatrix} \ln(\Delta B)^0 \\ \vdots \\ \ln(\Delta B)^n \end{bmatrix}\right) \tag{7}$$

It is important to mention that only values confined by the experimental data are used in this section. The mean error and the root mean square errors of the fitted curve are -0.004 % and 0.87 %, respectively. The maximum and minimum errors are 2.25 % and -3.28 %, respectively.

With a proper definition of the loss space, the CWH can be evaluated for data when $D \neq 0.5$. The core losses for each segment of the data available are evaluated separately following (7), and then the power losses are combined in accordance to (6). The results are shown in Fig. 4, where the data for each duty cycle is shown individually.

According to the results, the CWH satisfactorily predicts the losses in the space boundary defined. A mean error of -0.38 % and a root mean square error of 1.69 % is achieved. The maximum and minimum errors are 6.59 % and -6.13 %, respectively.

For comparison, a brief analysis of the CWH using the MagNet database is also presented in [13]. The paper focuses on the complexity of core loss quantification and does not go

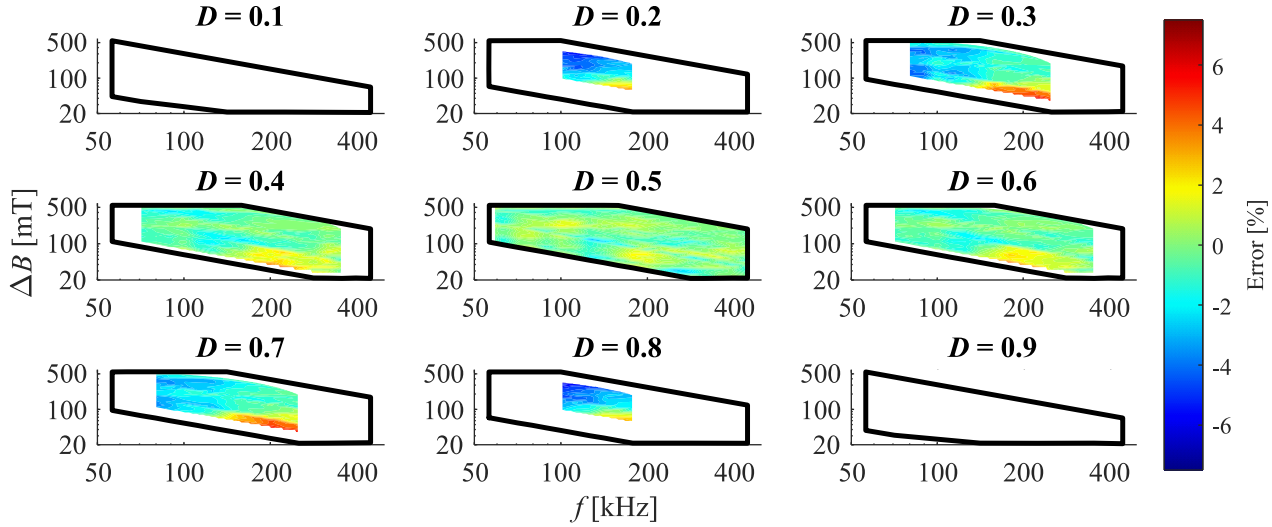

Fig. 4: Core loss prediction accuracy using the CWH for material N87 at 25 ºC and triangular waveforms for different duty cycles. The colored area represents the range where the CWH methodology can be applied while the black line represents the set of experimental data available from MagNet.

This article has been accepted for publication in IEEE Transactions on Power Electronics. This is the author's version which has not been fully edited and content may change prior to final publication. Citation information: DOI 10.1109/TPEL.2023.3323577

into depth detail of the CWH. Still, the results of the CWH methodology applied to predict losses for the same material at the same temperature when D = 0.8 are presented. [13] reports an average error of -2.4 % and a maximum discrepancy of 6.4 %. This properly correlates with the results achieved in this study when D = 0.8: an average error of -1.99 % and a maximum discrepancy of 6.13 %. The errors do not match exactly since [13] uses data interpolation to estimate the losses, and this work uses a fitting process to describe the loss space as (7).

Another key aspect of the results, which is also observable in Fig. 4 and the data presented in [13], is the restriction on the frequency and flux density ranges where the CWH approach is applicable imposed by the loss space boundary limit. This is expected due to the effect of duty cycle on the $|dB/dt|$ (8). Thus, the frequency range where the CWH is applicable decreases as the duty cycle approaches 0 or 1.

$$\left|\frac{dB}{dt}\right|_D = \frac{0.5}{D}\left|\frac{dB}{dt}\right|_{0.5} \tag{8}$$

In fact, considering the case of ΔB = 120 mT where data for the whole range $f \in$ [55, 445] kHz at D = 0.5 is available, only losses on the range of $f \in$ [88, 178] kHz at D = 0.8 (or D = 0.2) are evaluable, and at D = 0.9 (or D = 0.1) the range becomes $f \in$ [99, 89] = [Ø] kHz. Therefore, with the available data the CWH cannot be evaluated for D = 0.9 (or D = 0.1).

To quantify this limitation of the CWH, a Loss Space Coverage Ratio (*LSCR*) is defined as (9). The *LSCR* establishes the relation between the size of the data evaluable with the CWH and the size of the full data, by generating bounding polygons to both sets of data. Thus, the closer the *LSCR* is to 1 the higher the range where the CWH can be used.

$$LSCR = \frac{\text{area(CWH data set)}}{\text{area(full data set)}} \tag{9}$$

This is achieved by applying MATLAB's `boundary()` and `area()` functions to the data sets. The well-defined geometries from Fig. 4 ensure no ambiguity is introduced when defining bounding polygons. The *LSCR* values obtained are the following: $LSCR_{D=0.1}$ = 0.00, $LSCR_{D=0.2}$ = 0.15, $LSCR_{D=0.3}$ = 0.40, $LSCR_{D=0.4}$ = 0.69 and as expected $LSCR_{D=0.5}$ = 1.00. For $D \in$ [0.6, 0.9] the *LSCR* is symmetrical around D = 0.5. Thus, the overall $LSCR_{D\in[0.1,\ 0.9]}$ = 0.39, meaning that the CWH can only predict core losses in less than 40 % of the complete data set. To achieve a 100 % coverage of the complete data set, core losses for D = 0.5 waveforms in the frequency range of $f \in$ [30, 2225] kHz would be necessary. This frequency range increases even more drastically for $D \notin$ [0.1, 0.9].

The same can be observed in [7], where the variability of the α and β parameters is evaluated in the range of $f \approx$ [50, 1000] kHz. The results presented are at 100 kHz with $D \in$ [0.05, 0.95], which according to (8) would require a frequency range of $f \in$ [52, 1000] kHz.

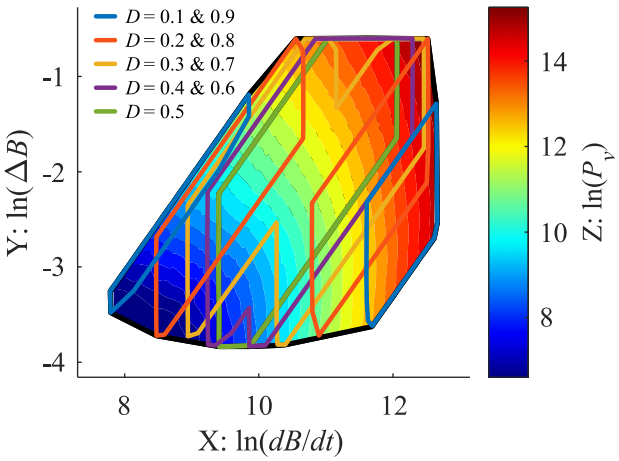

Fig. 5: Expanded loss space obtained from the MagNet data. The boundaries for the loss spaces expansions generated from each duty cycle are highlighted.

IV. Expanded Loss Space

Although the CWH clearly proves to be an adequate approach to estimate core losses on triangular waveforms for a wide range of duty cycle, the requirement of experimental data in a wide range of frequencies makes it impractical for very high and low duty cycles. This defeats the purpose of the improved accuracy regarding the commonly used approaches such as the iGSE.

Alternatively, instead of limiting the loss space to D = 0.5 data, the data from $D \neq$ 0.5 (Fig. 4) can be used to expand the loss space. In fact, recalling the definition of the CWH (6), the losses for the segment AA of the asymmetrical waveform AB can be deduced for known AB and BB losses. Thus, as long as one of the segments of an asymmetrical waveform is in the $|dB/dt|$ and ΔB ranges of the loss space, loss data for the other segment can be deduced from (10) for known P_{AB} losses.

$$P_{AA} = \frac{P_{AB} - (1-D)P_{BB}}{D} \tag{10}$$

In most cases, at least one of the segments of the MagNet data waveforms is inside the loss space boundary. Therefore, by combining the original loss space with the data generated from (10), an expanded loss space is generated. The steps to generate the expanded loss space are detailed in **APPENDIX A**.

This expanded loss space is shown in Fig. 5, where the data obtained from the different duty cycles is marked. Once again,

TABLE II
COEFFICIENTS FOR EXPANDED LOSS SPACE

	p_{n0}	p_{n1}	p_{n2}	p_{n3}	p_{n4}	p_{n5}
p_{0n}	-1289	-348.4	-7.212	5.698	0.4278	5.515E-3
p_{1n}	495.8	112.2	3.467	-0.7765	-0.03234	0
p_{2n}	-74.57	-13.21	-0.4079	0.02559	0	0
p_{3n}	5.523	0.6749	0.01416	0	0	0
p_{4n}	-0.2007	-0.01261	0	0	0	0
p_{5n}	2.864E-3	0	0	0	0	0

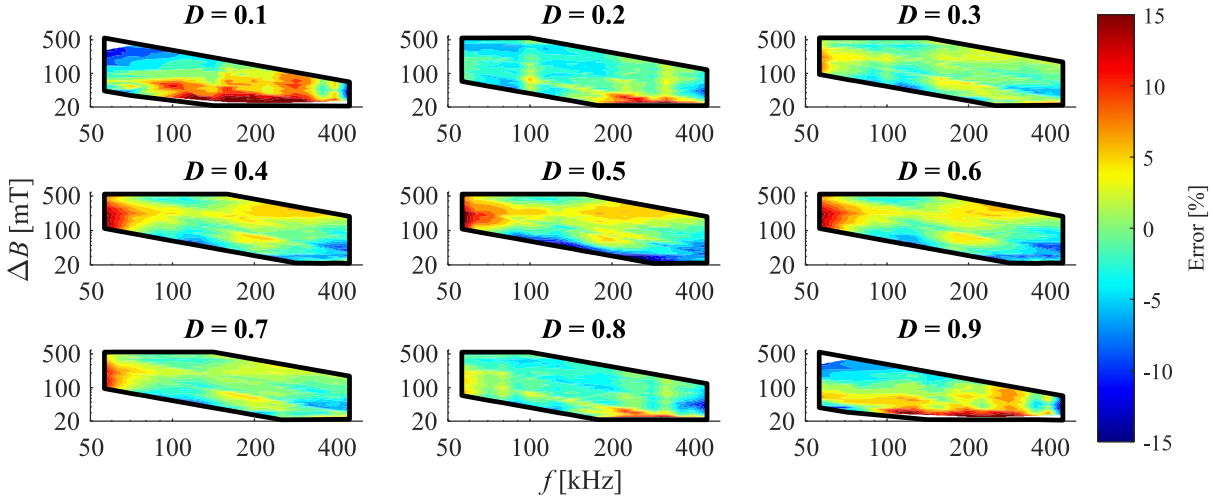

Fig. 6: Core loss prediction accuracy using the CWH with the expanded loss space for material N87 at 25 ºC and triangular waveforms for different duty cycles. The colored area represents the range where the expanded CWH methodology can be applied while the black line represents the set of experimental data available from MagNet.

the expanded loss space has been fitted into a polynomial surface of the fifth degree, so it can be defined by (7). The coefficients for this polynomial surface are recorded in TABLE II. Since the amount of data has been significantly increased, a worst fitting quality is achieved when compared to the initial loss space.

The results achieved by the expanded loss space are shown in Fig. 6. A first examination proves that the expanded loss space greatly increases the data range where the CWH is applicable. *LSCR* values of $LSCR_{D=0.1} = 0.90$, $LSCR_{D=0.2} = 0.96$, $LSCR_{D=0.3} = 0.99$, $LSCR_{D=0.4} = 1.00$ and $LSCR_{D=0.5} = 1.00$ are achieved. For $D \in [0.6, 0.9]$ the *LSCR* is also symmetrical around $D = 0.5$. Compared to the original loss space ($LSCR_{D\in[0.1, 0.9]} = 0.39$), the expanded loss space has an overall $LSCR_{D\in[0.1, 0.9]} = 0.97$.

As a tradeoff, the expanded loss space has an increased degree of error. In this case, a mean error of 0.44 % and a root mean square error of 2.57 % is achieved. The new maximum and minimum errors are 17.69 % and -8.62 % respectively. A more in detail analysis reveals that 99 % of the data (99 percentile) have absolute errors lower than 8.23 %.

All in all, for the MagNet data set studied (3312 data points), the expanded loss space greatly increases the range of the CWH approach for core loss prediction (from 1305 to 3234 data points), while retaining a high accuracy.

V. Connection With Steinmetz Parameters

As briefly discussed in the introduction, the most utilized technique for core loss prediction is the iGSE [4]. As demonstrated by the comparison of the iGSE and ISE, and the study realized in this work, the main factor increasing the discrepancy of the iGSE with experimental data is the assumption that equal Steinmetz parameters are applied to calculate the power losses produced by each segment of the waveform.

Thus, improved accuracy can be achieved with the iGSE if it is modified to follow the assumption (6) from the CWH. This modification could be referred as the composite improved Generalized Steinmetz Equation (ciGSE). For triangular waveforms, the ciGSE can be written as (11), where the Steinmetz parameters are treated individually for each segment of the waveform. Unfortunately, a low *LSCR* similar to the original loss space would be achieved for the ciGSE if the data range to extract the Steinmetz parameters (mainly the frequency) is not increased accordingly. Thus, sinusoidal loss data from $f \in [30, 2225]$ kHz would be necessary to evaluate the data range used in this study.

$$P_v = \sum_n D_n \cdot k_{i_n} \left|\frac{dB}{dt}\right|^{\alpha_n} \Delta B^{\beta_n - \alpha_n} \tag{11}$$

Alternatively, the Steinmetz parameters for triangular waveforms could be extracted from the expanded loss space presented in this work, since combining assumption (6) with (11) generates the definition (12) for power losses of the *n* segment. Additionally, this also avoids the error introduced from the transformation of sinusoidal losses into triangular losses intrinsic to the SE approaches. (12) can be rewritten as (13), while (7) can be rewritten as (14). Due to the equality of (13) and (14), and considering that the partial derivatives $\partial\ln(|dB/dt|)$ and $\partial\ln(\Delta B)$ of (13) develop into the definitions for α_n and β_n- α_n, these can be defined as (15) and (16).

$$P_{v_n} = k_{i_n} \left|\frac{dB}{dt}\right|^{\alpha_n} \Delta B^{\beta_n - \alpha_n} \tag{12}$$

$$\ln(P_{v_n}) = \ln(k_{i_n}) + \alpha_n \ln\left(\left|\frac{dB}{dt}\right|\right) + (\beta_n - \alpha_n)\ln(\Delta B) \tag{13}$$

$$\ln(P_{v_n}) = \begin{bmatrix} \ln\left(\left|\frac{dB}{dt}\right|\right)^0 & \cdots & \ln\left(\left|\frac{dB}{dt}\right|\right)^n \end{bmatrix} \times \begin{bmatrix} p_{00} & \cdots & p_{0n} \\ \vdots & \ddots & \vdots \\ p_{n0} & \cdots & p_{nn} \end{bmatrix} \times \begin{bmatrix} \ln(\Delta B)^0 \\ \vdots \\ \ln(\Delta B)^n \end{bmatrix} \tag{14}$$

This article has been accepted for publication in IEEE Transactions on Power Electronics. This is the author's version which has not been fully edited and content may change prior to final publication. Citation information: DOI 10.1109/TPEL.2023.3323577

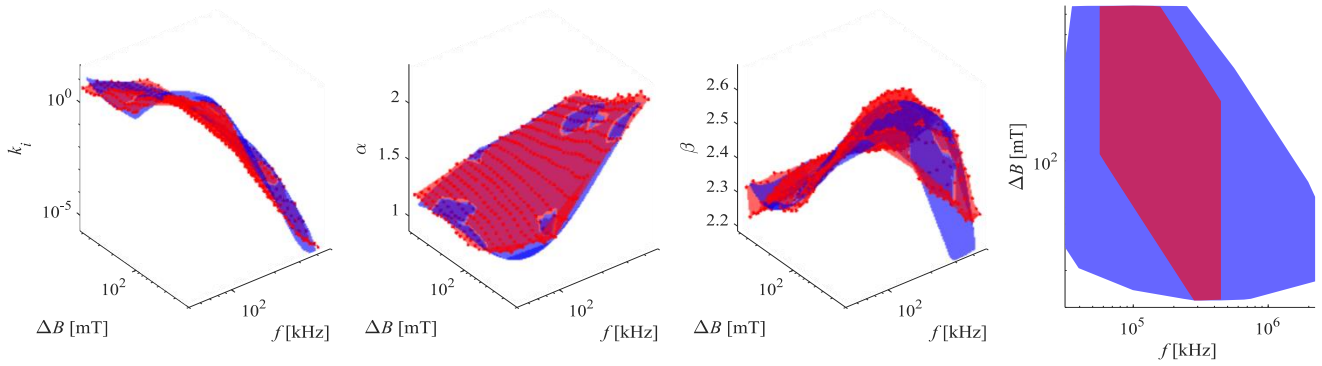

(a) (b) (c) (d)

Fig. 7: Steinmetz parameters (a) k_i, (b) α and (c) β obtained from the expanded loss space and approximated from local D = 0.5 loss data. (d) The data ranges for the Steinmetz parameters obtainable from the classical approach and derivable from the expanded loss space are also visualized.

$$\alpha_n = \begin{bmatrix} 0 & \cdots & n\ln\left(\left|\frac{dB}{dt}\right|\right)^{n-1} \end{bmatrix} \times \begin{bmatrix} p_{00} & \cdots & p_{0n} \\ \vdots & \ddots & \vdots \\ p_{n0} & \cdots & p_{nn} \end{bmatrix} \times \begin{bmatrix} \ln(\Delta B)^0 \\ \vdots \\ \ln(\Delta B)^n \end{bmatrix} \quad (15)$$

$$\beta_n - \alpha_n = \begin{bmatrix} \ln\left(\left|\frac{dB}{dt}\right|\right)^0 & \cdots & \ln\left(\left|\frac{dB}{dt}\right|\right)^n \end{bmatrix} \times \begin{bmatrix} p_{00} & \cdots & p_{0n} \\ \vdots & \ddots & \vdots \\ p_{n0} & \cdots & p_{nn} \end{bmatrix} \times \begin{bmatrix} 0 \\ \vdots \\ n\ln(\Delta B)^{n-1} \end{bmatrix} \quad (16)$$

With α_n and β_n defined, the k_{in} parameter can be solved by replacing the corresponding values in (12) or (13). A comparison between the iGSE parameters obtained from D = 0.5 triangular waveform data and the parameters obtained from the expanded loss space is shown in Fig. 7. Instead of evaluating the Steinmetz parameters in an extensive data range, the local values are obtained by evaluating the parameters in the f ± 25 % and ΔB ± 25 % ranges.

The definitions of k_i (Fig. 7a), α (Fig. 7b), and β (Fig. 7c) obtained from the expanded loss space match closely with the ones obtained from the iGSE. As shown in Fig. 7d, using the expanded loss space the Steinmetz parameters can be described in a much larger range than classical approaches.

Comparisons of power loss predictions with the iGSE and ciGSE at different frequencies and duty cycles are shown in Fig. 8. The local Steinmetz parameters extracted from D = 0.5 data are used for the iGSE, thus the results match perfectly at D = 0.5. The ciGSE is evaluated using the Steinmetz parameters extracted from the expanded loss space for each segment. The results clearly show how the iGSE struggles to accurately predict the losses for high and low duty cycles, while as expected from our analysis of the expanded loss space accuracy, the ciGSE is capable to model this behavior accurately. A more detailed demonstration of how to use the ciGSE is presented in **APPENDIX B**, where its compatibility with other works related to the topic is also discussed.

More details about the error distribution are shown in Fig. 9. Once again, the exact fitting of the iGSE from D = 0.5 is visible by the amount of data with an error of 0 %, but the error is higher when considering data of $D \neq 0.5$. Overall, the iGSE achieves a root mean square error of 15.01 %, with 90, 95 and 99 percentiles of 28.38 %, 37.80 % and 46.83 % respectively. For the iGSE, the root mean square error is 2.57 %, with 90, 95 and 99 percentiles of 4.00 %, 5.35 % and 8.23 %, respectively (same results from **Section IV**). The results prove that, for the core material N87 at 25 ºC, the proposed expanded loss space and ciGSE approach greatly increases accuracy, reducing the root mean square error and 95 percentiles by 5.85 and 6.96 times.

As expected, for D = 0.1 and D = 0.9 the improvement is more noticeable: the iGSE achieves a root mean square error and 95 percentile of 34.67 % and 48.12 %, while the ciGSE improves these values to 3.95 % and 7.89 %. This equates to an error reduction of 8.78 and 6.10 times.

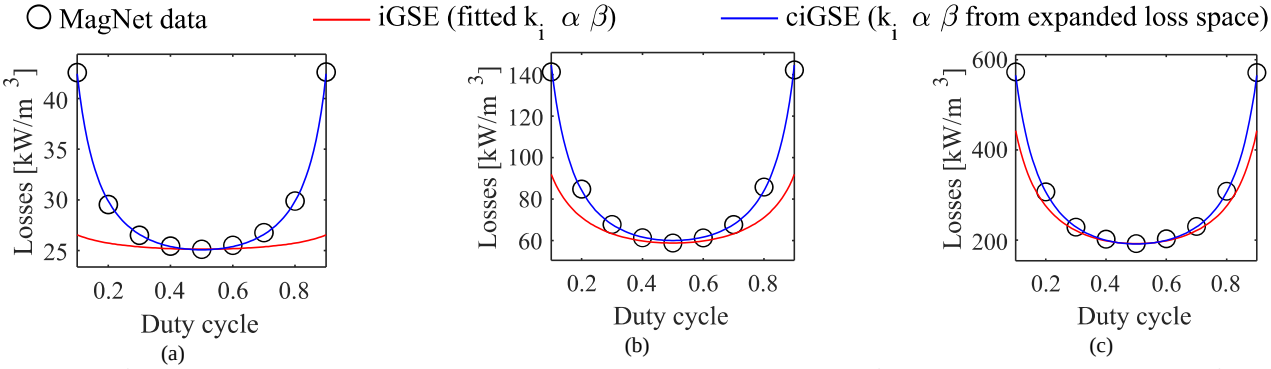

Fig. 8: Comparison of core loss prediction with the iGSE and the ciGSE with the experimental data available from MagNet. The losses presented are for (a) f = 100 kHz and ΔB = 100 mT, (b) f = 200 kHz and ΔB = 100 mT, and (c) f = 400 kHz and ΔB = 100 mT.

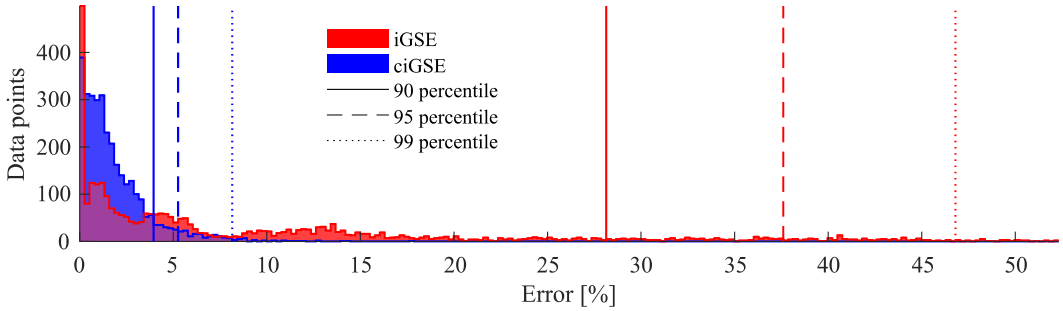

Fig. 9: Error distributions of the iGSE and ciGSE for N87 at 25ºC, : $f \in [55, 445]$ kHz, $\Delta B \in [20, 550]$ mT and $D \in [0.1, 0.9]$

VI. Validation For Other Materials

For now, only data for ferrite N87 material at 25 ºC has been studied (3312 data points). Note that the accuracy of the proposed methodology has only been tested in the data range bounded by the expanded loss space. To ensure the proposed methodology works not only in the conditions tested, data for triangular waveforms of different materials and temperatures must be tested. At the same time, an analysis of the error introduced by the extrapolation of the expanded loss space should be checked.

Thus, the new approach for core loss calculation proposed in this paper has been tested using the rest of the data available from MagNet. The database has available TDK EPCOS N87, N49, N30, N27, Ferroxcube 3C94, 3C90, 3E6, 3F4, and Fair-Rite 77 and 78 materials. Data at 25, 50, 70 and 90 ºC is available for each, adding up to 59423 data points (triangular waveforms without DC magnetization).

There are certain limitations on the validation process. Not all materials have equal amount of data points; N87, 3C94 and 3C90 all have at least 12627 (3C94) data points, while the rest of the materials have between 2045 (3E6) and 3542 (N27) points. There are also some caveats too with specific cases which will generate anomalous results in the validation process; one such example is the 3F4 material with $D = 0.1$, where very limited amounts of data is available across all temperatures (25 points) in comparison with $D = 0.9$ (176 points). Also, the frequency and flux density ranges used for the parametrization of the local Steinmetz parameters had to be increased from ± 25 % to ± 30 % to better accommodate the datasets of all materials.

The results of the analysis of different materials at different temperatures is presented in TABLE III. All the data available,

TABLE III
iGSE AND ciGSE ACCURACY FOR THE MAGNET DATABASE

Material	Temp. [ºC]	Error RMS [%]		Error 95 percentile [%]		Data points
		iGSE	ciGSE	iGSE	ciGSE	
N87	25	15,33	3,05	38,17	6,08	3312
	50	14,51	4,48	36,39	9,24	3299
	70	17,23	6,56	40,37	14,88	3304
	90	16,56	10,13	41,81	24,07	3275
N49	25	18,18	7,48	38,91	13,14	708
	50	37,63	13,78	53,63	15,43	682
	70	24,96	8,83	47,50	14,65	705
	90	18,72	10,72	39,95	12,68	744
N27	25	14,69	4,90	35,59	8,50	886
	50	20,01	8,84	42,41	14,52	888
	70	14,57	9,54	36,66	20,02	885
	90	14,10	11,02	31,00	23,29	883
3C94	25	14,75	11,49	33,37	17,21	3165
	50	16,18	13,41	38,68	19,49	3162
	70	16,01	9,07	35,78	16,79	3148
	90	18,48	10,54	43,65	23,40	3152
3C90	25	15,90	3,96	39,69	6,94	3302
	50	17,01	5,95	40,22	12,03	3286
	70	19,01	8,54	44,74	19,75	3273
	90	17,95	10,84	43,62	24,84	3262
3E6	25	8,47	16,44	17,34	34,19	515
	50	19,05	4,46	20,35	5,37	516
	70	9,78	35,32	18,86	26,37	512
	90	9,95	13,31	20,26	11,46	502
3F4	25	10,48	6,50	24,84	9,12	617
	50	14,48	9,99	34,26	12,29	573
	70	17,76	13,88	37,28	16,11	562
	90	19,17	9,59	40,66	12,73	562
77	25	15,66	6,30	36,03	10,00	883
	50	19,80	10,84	27,24	17,47	882
	70	14,48	13,14	37,31	27,35	884
	90	13,52	14,34	33,86	34,27	879
78	25	15,40	6,28	35,48	11,33	881
	50	19,15	8,81	38,61	19,99	880
	70	14,63	13,38	38,05	30,11	882
	90	11,97	13,17	29,61	31,33	881
N30	25	11,55	4,11	28,39	5,75	678
	50	14,05	6,76	34,35	8,82	678
	70	12,95	4,96	31,08	5,57	674
	90	10,21	23,20	23,60	11,64	661
OVERALL		**16,73**	**10,02**	**38,23**	**17,94**	**59423**

TABLE IV
iGSE AND ciGSE ACCURACY FOR THE MAGNET DATABASE INSIDE THE EXPANDED LOSS SPACE BOUNDARY

Material	Temp. [ºC]	Error RMS [%]		Error 95 percentile [%]		Data points
		iGSE	ciGSE	iGSE	ciGSE	
N87	25	15,01	2,57	37,75	5,35	3234
	50	14,12	4,02	35,83	8,68	3224
	70	16,07	6,03	38,10	13,08	3227
	90	15,85	9,65	40,54	22,52	3199
N49	25	14,10	4,06	33,25	7,13	662
	50	16,72	4,28	35,73	7,86	630
	70	18,10	4,07	43,67	7,34	656
	90	15,14	3,78	35,79	7,20	690
N27	25	13,54	2,37	34,13	4,91	817
	50	15,55	4,10	35,37	9,13	813
	70	12,95	5,96	32,78	13,78	811
	90	11,66	6,16	28,41	14,00	808
3C94	25	14,77	3,02	33,95	5,87	2956
	50	14,34	4,58	34,51	10,25	2958
	70	14,79	4,99	34,49	11,09	2944
	90	17,23	6,79	41,60	15,05	2947
3C90	25	15,28	2,71	38,96	5,70	3173
	50	15,67	4,52	38,33	9,46	3162
	70	17,32	7,21	41,89	16,42	3146
	90	17,60	9,04	43,32	20,90	3135
3E6	25	7,32	1,37	15,07	2,99	414
	50	7,79	1,58	17,11	3,35	409
	70	8,52	2,05	18,30	4,31	410
	90	9,32	2,08	20,80	4,10	404
3F4	25	9,53	3,57	20,96	6,50	588
	50	12,98	4,40	29,13	8,57	544
	70	11,15	4,65	26,20	8,69	519
	90	12,98	5,43	31,78	10,55	535
77	25	14,28	2,90	33,64	6,48	817
	50	15,44	4,57	32,65	9,45	816
	70	12,14	7,58	29,74	17,26	815
	90	11,50	8,64	27,92	20,12	816
78	25	15,50	3,06	33,40	6,41	814
	50	15,88	6,25	35,64	12,49	813
	70	12,20	8,72	31,65	21,25	812
	90	10,92	8,74	27,32	20,14	812
N30	25	9,47	1,43	22,91	3,01	579
	50	10,71	1,64	25,27	3,42	576
	70	10,09	2,04	23,07	4,07	572
	90	8,05	2,23	17,46	4,55	559
OVERALL		**14,85**	**5,63**	**35,93**	**12,60**	**55816**

This article has been accepted for publication in IEEE Transactions on Power Electronics. This is the author's version which has not been fully edited and content may change prior to final publication. Citation information: DOI 10.1109/TPEL.2023.3323577

even the points with segments outside of the expanded loss space are taken into account for these results. Overall, the iGSE achieves a root mean square error of 16.73 % while the ciGSE reduces this to 10.02 %. Similarly, the ciGSE reduces the 95 percentile from 38.23 % to 17.94 %. Note that there are some anomalous results in TABLE III, most noticeable in the results from material 3E6. The caveats presented above could explain these anomalies, although the extrapolation used to evaluate data outside of the expanded loss space boundaries also has a significant effect. Even then, for the shake of completion, the results reported in this section will refer to the overall errors considering all the materials and temperatures, even those with anomalous results.

The results obtained when the data is limited to the extended loss space boundary are displayed in TABLE IV. Not much difference between the results for the iGSE is noticeable in this case, the root mean square error and the 95 percentile have decreased to 14.85 % and 35.93 %, but the change is much more noticeable with the ciGSE, with errors of 5.63 % and 12.60 % respectively. As expected, the amount of data points analyzed when only data inside the loss space is tested is lower, from 59432 data points to 55816. Assuming a uniformly distributed data set, this would translate to an *LSCR* of roughly 94 %.

Note that until now the overall results for $D \in [0.1, 0.9]$ have been shown, but the main interest of this work is at $D \notin [0.3, 0.7]$, where the iGSE is unable to accurately predict the core losses. To represent how the accuracy of the model changes depending on the duty cycle, the errors for each value of D are represented individually in Fig. 10. As expected, the iGSE achieves perfect accuracy for $D = 0.5$, but the accuracy degrades as D increases or decreases. Meanwhile, the accuracy of the ciGSE is worst around $D = 0.5$ but is less deteriorated by the changes in D.

For $D \in [0.4, 0.6]$, the iGSE has a maximum RMS and 95 percentile error of 4.00 % and 5.01 % outperforming the 6.55 % and 13.60 % achieved by the ciGSE. On the contrary, the ciGSE outperforms the iGSE for $D \notin [0.4, 0.6]$. Starting from $D = 0.3$ and $D = 0.7$, the iGSE has RMS and 95 percentile errors of 6.86 % and 12.32 %, while the ciGSE achieves errors of 5.49 % and 10.62 % respectively. The discrepancy increases at $D = 0.1$ and $D = 0.9$, with 34.41 % and 53.92 % for the iGSE and 19.39 % and 38.72 % for the ciGSE.

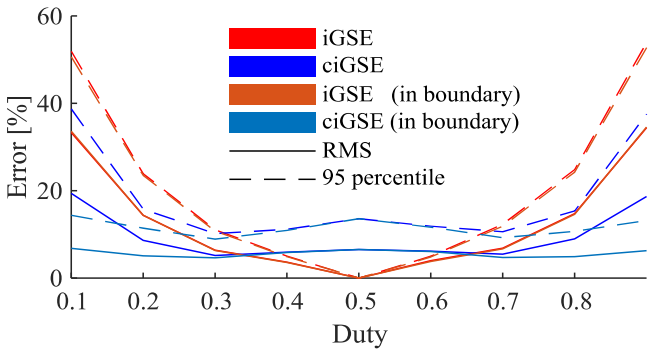

Fig. 10: Root mean square and 95 percentile errors of the iGSE and ciGSE for different duty cycles.

The quality of the ciGSE is closely connected to the methodology used to generate the expanded loss space. Due to the density of the experimental data being lowest at $D = 0.1$, $D = 0.5$, and $D = 0.9$ (Fig. 5), the errors for these points are higher. Future work should incorporate a weighted regression, taking into account this uneven data density, to model the expanded loss space with higher accuracy.

In addition, Fig. 10 also shows the results when the evaluation data is limited to the expanded loss space boundary, where extrapolation is avoided. In this case, for $D \in [0.4, 0.6]$, the iGSE has a maximum RMS and 95 percentile error of 3.78% and 4.89 %, outperforming the 6.10 % and 11.65 % achieved by the ciGSE. On the contrary, the ciGSE outperforms the iGSE for $D \notin [0.4, 0.6]$. Starting from $D = 0.3$ and $D = 0.7$, the iGSE has RMS and 95 percentile errors of 6.67 % and 11.89 %, while the ciGSE achieves errors of 4.73 % and 9.26 % respectively. The discrepancy increases at $D = 0.1$ and $D = 0.9$, with 34.56 % and 52.77 % for the iGSE and 6.80 % and 14.39 % for the ciGSE.

While no noticeable changes occur for the iGSE inside or outside the expanded loss space boundaries, it is clear that the ciGSE achieves much better results when extrapolation is not necessary. This discrepancy directly connects to the approach used to model the expanded loss space: the fifth degree polynomial surface used in this work is accurate inside the evaluated boundaries, but non-optimal for data extrapolation. Other approaches to model the loss space, such as a double exponential function (17) like the original concept proposed by Charles Proteus Steinmetz [14] (serving as inspiration for the SE) or the one proposed in DNSE [5], can serve to improve the performance of the model outside of these boundaries. Bézier curves or similar approaches also avoid problems generated by the extrapolation [15], [16].

$$P_v = c_1 \left|\frac{dB}{dt}\right|^{c_2} \Delta B^{c_3} + c_4 \left|\frac{dB}{dt}\right|^{c_5} \Delta B^{c_6} \tag{17}$$

Lastly, the impact of the temperature in the accuracy of the iGSE and ciGSE is also studied. Results for the overall errors at each temperature are presented in Fig. 11. The accuracy of the iGSE is mostly unaffected by the temperature, with RMS and 95 percentile errors of 15.62 % and 38.16 % at 25 ºC, and 16.61 % and 40.30 % at 90 ºC. On the opposite, the accuracy of the ciGSE is heavily influenced by the core temperature, with

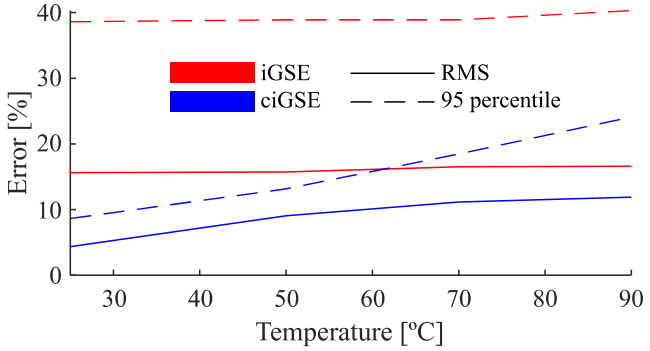

Fig. 11: Root mean square and 95 percentile errors of the iGSE and ciGSE for different temperature values.

errors of 5.45 % and 8.64 % at 25 ºC increasing to 11.89 % and 24.09 % at 90 ºC. An in-depth analysis of the dependency of the expanded loss space on temperature could potentially improve the modern understanding of the effect of temperature in the core loss mechanisms.

VII. Conclusion

This paper presents a complete study of the CWH [6] in the prediction of core losses using the experimental data available from the MagNet database [9]-[12]. An explanation of the original CWH and its application to the N87 material at 25 ºC is presented. Although only applicable in a limited range (< 40 % of the data), the high accuracy (E_{RMS} = 1.69 %, $|E|_{MAX}$ = 6.89 %) of the CWH is proven.

To overcome this limitation, the expanded loss space is developed, increasing the applicable range (from 40 % to 97 %) while retaining a high accuracy (E_{RMS} = 2.57 %, $|E|_{MAX}$ = 17.69 %). The expanded loss space allows predicting the losses under low and high duty cycles more accurately than the commonly used iGSE [4].

Next, the relation between the expanded loss space and the Steinmetz parameters employed in the iGSE is demonstrated. A because of this, it is decided to call the developed model the ciGSE, combining the core ideas of each approach: the calculation of the losses of each segment separately (CWH) and the definition of losses as functions of $|dB/dt|$ and ΔB (iGSE). An accuracy analysis for the studied case (N87 at 25 ºC, 3312 data points) demonstrates that the ciGSE can improve the RMS and 95 percentile errors by 5.85 and 6.96 times.

Lastly, the new methodology presented in this work is applied to the rest of the materials and temperatures available from the MagNet database (59423 data points). Detailed results of the effects of duty cycle and temperature in the accuracies of both approaches are presented and discussed. The results prove that the model is capable of properly predicting the losses for low and high duty cycles with other materials and temperatures. In addition, limitations of the extrapolation of losses due to the fitting equations used in this study are pointed out and future improvements proposed.

Acknowledgments

The authors would like to thank all people behind the generation and maintenance of the MagNet database.

Data Availability

All the experimental data used to support this study is available at MagNet [9]-[12].

Appendix A
Generation of the Expanded Loss Space

The generation of the expanded loss space is very similar to that of the classical loss space. The necessary steps to do so (Fig. 12) in MATLAB are detailed in this section, but this can also be implemented in any other programming environment if the main concepts are correctly implemented.

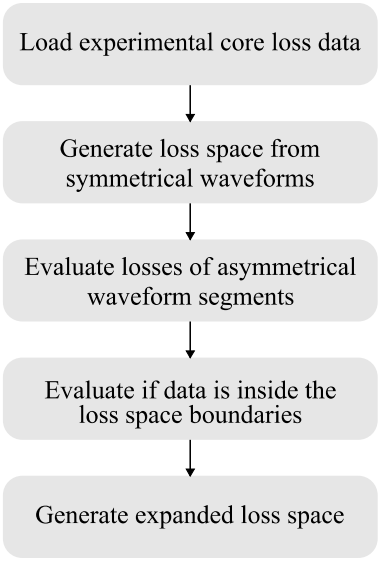

Fig. 12: Flow chart for the generation of the expanded loss space.

To generate the expanded loss space, first of all, the classical loss space using D = 0.5 is necessary. To do so, in this work the core loss data obtained from the MagNet database is organized in 4 arrays defining the peak to peak flux density, frequency, power losses and duty cycle (`DB`, `F`, `PAB` and `D`). From this data the values of $|dB/dt|$, ΔB and P_v necessary for the loss spaces can be directly evaluated (`dBdtA` and `dBdtB`, `DB` and `PAB`). For D = 0.5 both segments of the waveforms are the same, thus the non-expanded loss space is created using the `fit()` function as:

```
dBdtA=DB.*F./D
dBdtB=DB.*F./(1-D)
fitX=log(dBdtA(D==0.5))
fitY=log(DB(D==0.5))
fitZ=log(PAB(D==0.5))
LossSpace=fit([fitX',fitY'],fitZ','poly55')
```

Now, the losses for data points of $D \neq 0.5$ can be evaluated. The necessary data points for the expanded loss space according to (10) can be obtained from this loss space, which are the P_{AA} or P_{BB} losses obtained from P_{AB} and P_{BB} or P_{AA} respectively. The P_{BB} or P_{AA} must be inside the loss space boundaries (shown in Fig. 3) to avoid extrapolation during the extraction of the data points required for the expanded loss space. To do so, in this work the `boundary()` and `inpolygon()` functions are used to check if the data is inside the loss space boundaries (`iA` or `iB`):

```
PB=exp(LossSpace(log(dBdtA),log(DB)))
PA=exp(LossSpace(log(dBdtB),log(DB)))
PA_=(PAB-(1-D).*PA)./D
PB_=(PAB-D.*PB)./(1-D)
b=boundary(fitX',fitY',0.2)
iA=inpolygon(log(dBdtA),log(DB),fitX(b),fitY(b))
iB=inpolygon(log(dBdtB),log(DB),fitX(b),fitY(b))
```

Once the necessary data points are obtained, the expanded loss space is parametrized from the power losses of the segments generated from the non-expanded loss space:

```
fitX=log([dBdtB(iA),dBdtA(iB)])
fitY=log([DB(iA),DB(iB)])
fitZ=log([PB_(iA),PA_(iB)])
ExpandedSpace=fit([fitX',fitY'],fitZ','poly55')
```

Due to the randomness used by MATLAB when setting the initial values used by the `fit()`, slightly different coefficients might results for the same data set. A shrink factor of 0.2 was used for the `boundary()` function since it was seen to fit the available MagNet data correctly. Different shrink values might be necessary for other experimental datasets depending in the data distribution.

APPENDIX B
HOW TO USE THE PROPOSED METHODOLOGY

There are different ways to use the ciGSE. One can directly evaluate the losses of the segments of the waveform of interest using the expanded loss space, since it has been demonstrated that they are related with the Steinmetz parameters. The concept of the expanded loss space is presented in **Section IV**, while the details on how to generate it are shown in **APPENDIX A**. Thus, for any triangular waveform, the duty cycles of the segments AA and BB are D and (1-D) respectively (`DA` and `DB`), while the values of ΔB of both segments (`DB_A` and `DB_B`) is the same. Then, for a given frequency (`F`) the losses for each segment (`P_n`) and the total losses (`P_t`) can be evaluated according to (6).

If steps from **APPENDIX A** are followerd and the expanded loss space is already defined as a MATLAB surfacefit object (`sfit` type), the losses can be evaluated as:

```
D_n=[D_A,D_B]
DB_n=[DB_A,DB_B]
dBdt_n=DB_n.*F./DB_n
P_n=exp(ExpandedSpace(log(dBdtB_n),log(DB_n)))
P_t=sum(P_n.*D_n)
```

If this is not the case, (7) also can be used to evaluate the losses for each segment (`P_n`), and the total losses can be calculated in the same way. All the expanded loss space coefficients necessary to evaluate the losses using (7) can be found in TABLE V.

Alternatively, one can use the Steinmetz parameters extracted from the expanded loss space using (16) and (17) in combination with (11) to evaluate the total losses. This approach is more cumbersome then the other options, since the expanded loss space must first be transformer to Steinmetz parameters and then these must be used to evaluate the losses. Still, since this approach is related to the classical Steinmetz parameters and connected to the iGSE, it can potentially be combined with other works that build on the iGSE, such as the SPG [17] and related works [18] and to evaluate losses under DC bias conditions, and the i^{2}GSE [19] to evaluate the impact of relaxation losses.

REFERENCES

[1] S. A. Mulder, "Fit Formulae for Power Loss in Ferrites and their Use in Transformer Design," in proc. *26th International Power Conversion Conference (PCIM)*, 1993.

[2] J. Reinert, A. Brockmeyer, R. W. A. A. De Doncker, "Calculation of losses in ferro- and ferrimagnetic materials based on the modified Steinmetz equation," *IEEE Transactions on Industry Applications*, Volume 37, Issue 4, 2001.

[3] J. Li, T. Abdallah, C. R. Sullivan, "Improved calculation of core loss with nonsinusoidal waveforms," in proc. *2001 IEEE Industry Applications Conference*, 2001.

[4] K. Venkatachalam et al, "Accurate prediction of ferrite core loss with nonsinusoidal waveforms using only Steinmetz parameters," in proc. *IEEE Workshop Compututers in Power Electronics*, 2002.

[5] A. P. Van den Bossche, D. M. Van de Sype, V. C. Valchev, "Ferrite Loss Measurement and Models in Half Bridge and Full Bridge Waveforms," in proc. *IEEE Power Electronics Specialists Conference*, 2005.

[6] C. R. Sullivan, J. H. Harris, E. Herbert, "Core loss predictions for general PWM waveforms from a simplified set of measured data," in proc. *IEEE Applied Power Electrononics Conference and Exposition (APEC)*, 2010.

[7] S. Barg, K. Ammous, H. Mejbri, A. Ammous, "An Improved Empirical Formulation for Magnetic Core Losses Estimation Under Nonsinusoidal Induction," *IEEE Transactions on Power Electronics*, Volume 2, Issue 3, 2017.

[8] W. Shen, F. Wang, D. Boroyevich, C. W. Tipton, "Loss Characterization and Calculation of Nanocrystalline Cores for High-frequency Magnetics Applications," in proc. *IEEE Applied Power Electronics Conference and Exposition (APEC)*, 2007.

[9] D. Serrano et al., "Neural Network as Datasheet: Modeling B-H Loops of Power Magnetics with Sequence-to-Sequence LSTM Encoder-Decoder Architecture," in proc. *Workshop on Control and Modelling for Power Electronics (COMPEL)*, 2022.

[10] H. Li et al, "MagNet: An Open-Source Database for Data-Driven Magnetic Core Loss Modeling," in proc. *IEEE Applied Power Electronics Conference and Exposition (APEC)*, 2022.

[11] E. Dogariu et al, "Transfer Learning Methods for Magnetic Core Loss Modeling," in proc. *IEEE Workshop on Control and Modelling of Power Electronics (COMPEL)*, 2021.

[12] H. Li et al, "MagNet: A Machine Learning Framework for Magnetic Core Loss Modeling," in proc. *IEEE Workshop on Control and Modelling of Power Electronics (COMPEL)*, 2020.

[13] D. Serrano et al, "Quantifying the Complexity of Modeling Power Magnetic Material Characteristics," TechRxiv. Preprint.

[14] C. P. Steinmetz, "On the Law of Hysteresis," *Trans. AIEE*, Volume 9, Issue 2, 1892.

[15] J. M. Lane, R. F. Riesenfeld, "A Theoretical Development for the Computer Generation and Display of Piecewise Polynomial Surfaces", *IEEE Transactions on Pattern Analysis and Machine Intelligence*, Volume PAMI-2, Issue 1, 1980.

[16] P. Constantini, "Curve and Surface Construction Using variable Degree Polynomial Splines," *Computer Aided Geometric Design*, Colume 17, Issue 5, 2000.

[17] J. Muhlethaler, J. Biela, J. W. Kolar and A. Ecklebe, "Core Losses Under the DC Bias Condition Based on Steinmetz Parameters," in *IEEE Transactions on Power Electronics*, vol. 27, no. 2, pp. 953-963, Feb. 2012, doi: 10.1109/TPEL.2011.2160971.

[18] B. N. Sanusi et al, "Investigation and Modeling of DC Bias Impact on Core Losses at High Frequency," in *IEEE Transactions on Power Electronics*, vol. 38, no. 6, pp. 7444-7458, June 2023, doi: 10.1109/TPEL.2023.3249106.

[19] J. Mühlethaler, J. Biela, J. W. Kolar and A. Ecklebe, "Improved core loss calculation for magnetic components employed in power electronic system," 2011 Twenty-Sixth Annual IEEE Applied Power Electronics Conference and Exposition (APEC), Fort Worth, TX, USA, 2011, pp. 1729-1736, doi: 10.1109/APEC.2011.5744829.

TABLE V
COEFFICIENTS FOR THE EXPANDED LOSS SPACES OF ALL MATERIALS CURRENTLY AVAILABLE IN THE MAGNET DATABASE

Mat	Temp [°C]	p00	p10	p01	p20	p11	p02	p30	p21	p12	p03	p40	p31	p22	p13	p04	p50	p41	p32	p23	p14	p05
N87	25	-1.29E+03	4.96E+02	-3.48E+02	-7.46E+01	1.12E+02	-7.21E+00	5.52E+00	-1.32E+01	3.47E+00	5.70E+00	-2.01E-01	6.75E-01	-4.08E-01	-7.76E-01	4.28E-01	2.86E-03	-1.26E-02	1.42E-02	2.56E-02	-3.23E-02	5.52E-03
	50	-3.75E+03	1.36E+03	-1.74E+03	-1.91E+02	5.30E+02	-2.40E+02	1.30E+01	-6.00E+01	5.75E+01	-9.84E+00	-4.23E-01	2.98E+00	-4.58E+00	1.62E+00	-1.16E-02	5.13E-03	-5.48E-02	1.22E-01	-6.52E-02	5.70E-03	7.23E-03
	70	-4.87E+03	1.72E+03	-2.64E+03	-2.36E+02	7.81E+02	-4.70E+02	1.56E+01	-8.53E+01	1.08E+02	-3.09E+01	-4.94E-01	4.08E+00	-8.26E+00	4.77E+00	-8.09E-01	5.78E-03	-7.20E-02	2.09E-01	-1.87E-01	5.50E-02	-1.28E-02
	90	-1.17E+04	4.32E+03	-5.73E+03	-6.28E+02	1.74E+03	-9.70E+02	4.48E+01	-1.98E+02	2.17E+02	-8.11E+01	-1.55E+00	1.00E+01	-1.60E+01	1.24E+01	-2.73E+00	2.07E-02	-1.91E-01	3.91E-01	-4.76E-01	2.00E-01	-3.91E-02
N49	25	-2.14E+03	7.97E+02	-8.03E+02	-1.18E+02	2.27E+02	-1.26E+02	8.89E+00	-2.30E+01	3.37E+01	8.15E+00	-3.39E-01	9.67E-01	-2.94E+00	-9.46E-01	1.01E+00	5.31E-03	-1.36E-02	8.39E-02	2.17E-02	-7.87E-02	1.21E-02
	50	-3.66E+03	1.37E+03	-1.30E+03	-2.04E+02	3.87E+02	-1.31E+02	1.52E+01	-4.24E+01	3.63E+01	1.61E+01	-5.70E-01	2.02E+00	-3.24E+00	-1.90E+00	1.91E+00	8.60E-03	-3.50E-02	9.24E-02	4.37E-02	-1.55E-01	2.00E-02
	70	-3.32E+03	1.23E+03	-1.17E+03	-1.81E+02	3.40E+02	-1.28E+02	1.34E+01	-3.62E+01	3.57E+01	1.63E+01	-4.98E-01	1.65E+00	-3.18E+00	-1.84E+00	2.07E+00	7.49E-03	-2.68E-02	9.01E-02	3.95E-02	-1.59E-01	3.47E-02
	90	-2.50E+03	9.64E+02	-5.22E+02	-1.49E+02	1.50E+02	-2.04E+01	1.15E+01	-1.55E+01	8.99E+00	1.67E+01	-4.52E-01	6.64E-01	-1.03E+00	-2.25E+00	1.37E+00	7.19E-03	-9.73E-03	3.36E-02	6.65E-02	-1.16E-01	9.33E-03
N27	25	-2.72E+03	1.03E+03	-8.53E+02	-1.55E+02	2.57E+02	-8.86E+01	1.17E+01	-2.87E+01	2.15E+01	-3.38E-01	-4.38E-01	1.40E+00	-1.71E+00	1.54E-01	2.35E-01	6.57E-03	-2.52E-02	4.55E-02	-8.13E-03	-1.19E-02	8.56E-03
	50	-5.09E+03	1.90E+03	-2.13E+03	-2.83E+02	6.28E+02	-3.45E+02	2.11E+01	-6.84E+01	7.97E+01	-1.87E+01	-7.88E-01	3.26E+00	-6.17E+00	2.74E+00	-5.94E-01	1.19E-02	-5.69E-02	1.60E-01	-9.98E-02	4.46E-02	-6.58E-03
	70	-5.08E+02	-4.99E+01	-2.04E+03	4.56E+01	5.44E+02	-5.55E+02	-6.34E+00	-5.20E+01	1.24E+02	-4.24E+01	3.47E-01	2.07E+00	-9.17E+00	6.47E+00	-1.14E+00	-6.78E-03	-2.75E-02	2.24E-01	-2.48E-01	8.45E-02	-8.73E-03
	90	-1.81E+03	5.51E+02	-1.96E+03	-6.38E+01	5.19E+02	-5.75E+02	3.50E+00	-4.97E+01	1.25E+02	-5.35E+01	-8.98E-02	2.00E+00	-8.97E+00	7.85E+00	-1.96E+00	8.74E-04	-2.75E-02	2.14E-01	-2.90E-01	1.41E-01	-2.15E-02
3C94	25	-7.37E+02	3.21E+02	1.24E+02	-5.38E+01	-2.44E+01	1.03E+02	4.45E+00	1.59E+00	-2.05E+01	1.78E+01	-1.82E-01	-3.61E-02	1.32E+00	-2.59E+00	9.22E-01	2.95E-03	1.65E-04	-2.73E-02	9.23E-02	-7.32E-02	8.31E-03
	50	-4.06E+03	1.47E+03	-2.07E+03	-2.10E+02	6.30E+02	-3.06E+02	1.47E+01	-7.09E+01	7.49E+01	-8.47E+00	-5.03E-01	3.49E+00	-6.09E+00	1.40E+00	7.79E-02	6.68E-03	-6.30E-02	1.65E-01	-6.05E-02	-1.34E-02	-4.22E-03
	70	-4.89E+02	-6.47E+01	-1.93E+03	5.42E+01	5.57E+02	-4.44E+02	-7.97E+00	-5.95E+01	1.00E+02	-3.49E+01	4.69E-01	2.78E+00	-7.48E+00	5.47E+00	-8.11E-01	-1.00E-02	-4.80E-02	1.83E-01	-2.16E-01	6.05E-02	-3.97E-03
	90	6.00E+02	-6.30E+02	-2.46E+03	1.67E+02	7.17E+02	-5.83E+02	-1.90E+01	-7.79E+01	1.27E+02	-5.94E+01	9.98E-01	3.75E+00	-9.22E+00	8.73E+00	-2.54E+00	-2.00E-02	-6.75E-02	2.20E-01	-3.25E-01	1.75E-01	-4.84E-02
3C90	25	-9.21E+02	3.50E+02	-1.79E+02	-5.17E+01	5.95E+01	2.50E+01	3.73E+00	-7.00E+00	-3.74E+00	9.20E+00	-1.32E-01	3.50E-01	1.39E-01	-1.27E+00	6.28E-01	1.80E-03	-6.26E-03	2.25E-05	4.29E-02	-4.72E-02	9.30E-03
	50	-3.50E+03	1.22E+03	-1.90E+03	-1.63E+02	5.66E+02	-2.95E+02	1.05E+01	-6.22E+01	7.01E+01	-1.24E+01	-3.13E-01	2.98E+00	-5.58E+00	1.85E+00	-2.32E-01	3.32E-03	-5.21E-02	1.49E-01	-7.12E-02	1.15E-02	-4.93E-03
	70	-7.07E+03	2.56E+03	-3.69E+03	-3.64E+02	1.10E+03	-6.50E+02	2.55E+01	-1.22E+02	1.47E+02	-4.69E+01	-8.72E-01	5.96E+00	-1.10E+01	7.35E+00	-1.07E+00	1.15E-02	-1.09E-01	2.70E-01	-2.94E-01	6.91E-02	-1.79E-02
	90	-4.56E+03	1.36E+03	-4.14E+03	-1.41E+02	1.20E+03	-8.65E+02	4.86E+00	-1.31E+02	1.89E+02	-8.06E+01	7.39E-02	6.31E+00	-1.36E+01	1.21E+01	-2.87E+00	-5.73E-03	-1.14E-01	3.20E-01	-4.61E-01	1.98E-01	-4.79E-02
3E6	25	6.29E+01	7.98E+00	1.66E+02	-4.83E+00	-3.31E+01	7.29E+01	6.08E-01	2.58E+00	-9.67E+00	2.15E+01	-3.10E-02	-9.57E-02	4.03E-01	-2.00E+00	3.03E+00	5.81E-04	1.50E-03	-4.51E-03	4.80E-02	-1.40E-01	1.64E-01
	50	1.45E+03	-5.27E+02	4.89E+02	7.66E+01	-1.48E+02	4.25E+01	-5.52E+00	1.70E+01	-8.76E+00	3.08E+00	1.97E-01	-8.80E-01	6.11E-01	-3.75E-01	2.04E-01	-2.77E-03	1.72E-02	-1.40E-02	1.37E-02	-6.55E-03	1.03E-02
	70	2.16E+03	-8.00E+02	7.46E+02	1.18E+02	-2.37E+02	4.54E+01	-8.55E+00	2.82E+01	-1.23E+01	-3.87E+00	3.06E-01	-1.48E+00	1.07E+00	4.15E-01	-5.33E-01	-4.29E-03	2.93E-02	-2.91E-02	-5.48E-03	4.45E-02	-1.02E-02
	90	-1.89E+02	7.46E+01	-2.31E+01	-1.13E+01	7.55E+00	1.18E+01	8.83E-01	-3.95E-01	8.11E-01	1.02E+01	-3.58E-02	-2.16E-02	-2.12E-01	-8.39E-01	1.66E+00	6.17E-04	1.50E-03	7.61E-03	1.33E-02	-9.14E-02	6.40E-02
3F4	25	-6.87E+03	3.00E+03	-1.16E+03	-5.21E+02	4.16E+02	-1.69E+01	4.52E+01	-5.50E+01	9.49E+00	9.21E+00	-1.96E+00	3.18E+00	-1.21E+00	-1.36E+00	3.13E-01	3.40E-02	-6.81E-02	4.43E-02	4.55E-02	-3.89E-02	-1.76E-02
	50	-1.19E+04	5.04E+03	-2.62E+03	-8.48E+02	9.17E+02	-9.73E+01	7.11E+01	-1.19E+02	3.39E+01	1.45E+01	-2.97E+00	6.77E+00	-3.63E+00	-2.19E+00	5.37E-01	4.97E-02	-1.43E-01	1.23E-01	7.93E-02	-5.15E-02	-1.04E-02
	70	-1.21E+04	5.08E+03	-2.79E+03	-8.46E+02	9.88E+02	-6.94E+01	7.01E+01	-1.29E+02	3.02E+01	2.30E+01	-2.89E+00	7.39E+00	-3.49E+00	-3.11E+00	1.40E+00	4.74E-02	-1.57E-01	1.21E-01	9.71E-02	-1.19E-01	7.46E-04
	90	-1.40E+04	5.71E+03	-3.77E+03	-9.29E+02	1.27E+03	-2.37E+02	7.54E+01	-1.59E+02	7.17E+01	1.72E+01	-3.05E+00	8.73E+00	-6.90E+00	-2.05E+00	1.52E+00	4.93E-02	-1.78E-01	2.14E-01	5.08E-02	-1.19E-01	1.58E-02
77	25	-3.00E+03	1.13E+03	-1.07E+03	-1.68E+02	3.26E+02	-1.20E+02	1.24E+01	-3.67E+01	2.97E+01	-8.40E-01	-4.54E-01	1.81E+00	-2.42E+00	2.84E-01	2.83E-01	6.65E-03	-3.28E-02	6.55E-02	-1.46E-02	-1.35E-02	1.09E-02
	50	-4.34E+03	1.58E+03	-2.16E+03	-2.27E+02	6.32E+02	-3.76E+02	1.63E+01	-6.80E+01	8.84E+01	-1.87E+01	-5.82E-01	3.17E+00	-6.96E+00	2.77E+00	-5.98E-01	8.41E-03	-5.33E-02	1.84E-01	-1.01E-01	4.62E-02	-6.39E-03
	70	7.18E+03	-3.17E+03	-5.92E+02	5.54E+02	9.14E+01	-4.31E+02	-4.79E+01	6.46E-01	9.37E+01	-4.01E+01	2.05E+00	-6.29E-01	-6.61E+00	6.48E+00	-6.03E-01	-3.48E-02	2.36E-02	1.50E-01	-2.59E-01	6.06E-02	1.92E-02
	90	1.56E+04	-6.28E+03	2.96E+03	1.01E+03	-1.00E+03	-3.40E+01	-8.03E+01	1.26E+02	-4.71E+00	-3.38E+01	3.20E+00	-6.94E+00	1.40E+00	4.91E+00	-1.43E+00	-5.09E-02	1.42E-01	-6.42E-02	-1.77E-01	1.14E-01	-2.89E-03
78	25	-3.54E+03	1.32E+03	-1.37E+03	-1.95E+02	4.13E+02	-1.78E+02	1.43E+01	-4.61E+01	4.18E+01	-6.59E+00	-5.19E-01	2.27E+00	-3.27E+00	1.05E+00	-1.26E-02	7.51E-03	-4.12E-02	8.54E-02	-4.05E-02	5.34E-03	4.89E-03
	50	5.19E+02	-5.79E+02	-2.12E+03	1.53E+02	5.86E+02	-4.87E+02	-1.69E+01	-5.88E+01	1.11E+02	-3.16E+01	8.65E-01	2.50E+00	-8.40E+00	4.89E+00	-7.27E-01	-1.68E-02	-3.71E-02	2.11E-01	-1.90E-01	5.52E-02	-4.22E-03
	70	9.41E+03	-4.00E+03	3.51E+02	6.77E+02	-2.07E+02	-3.42E+02	-5.69E+01	3.57E+01	6.86E+01	-4.48E+01	2.38E+00	-2.43E+00	-4.38E+00	6.78E+00	-1.40E+00	-3.95E-02	5.80E-02	8.71E-02	-2.55E-01	1.14E-01	3.91E-04
	90	1.29E+04	-5.25E+03	2.05E+03	8.51E+02	-7.37E+02	-1.64E+02	-6.87E+01	9.72E+01	2.40E+01	-4.30E+01	2.76E+00	-5.59E+00	-7.69E-01	6.00E+00	-2.13E+00	-4.42E-02	1.19E-01	-8.55E-03	-2.10E-01	1.52E-01	-2.90E-02
N30	25	-2.01E+02	7.03E+01	-3.49E+02	-1.01E+01	7.87E+01	-1.85E+02	7.79E-01	-6.32E+00	3.44E+01	-3.13E+01	-3.10E-02	2.08E-01	-2.10E+00	3.99E+00	-2.16E+00	5.07E-04	-2.11E-03	4.29E-02	-1.21E-01	1.55E-01	-3.57E-02
	50	-1.50E+01	-3.47E+01	-4.87E+02	1.11E+01	1.17E+02	-2.00E+02	-1.23E+00	-1.01E+01	3.90E+01	-2.74E+01	6.00E-02	3.61E-01	-2.50E+00	3.74E+00	-1.39E+00	-1.09E-03	-4.30E-03	5.34E-02	-1.20E-01	1.17E-01	-3.04E-04
	70	6.67E+02	-2.80E+02	-1.31E+02	4.61E+01	1.16E+01	-1.36E+02	-3.69E+00	1.39E+00	2.36E+01	-2.51E+01	1.45E-01	-1.85E-01	-1.33E+00	3.08E+00	-1.81E+00	-2.25E-03	5.43E-03	2.50E-02	-8.81E-02	1.29E-01	-3.10E-02
	90	2.72E+02	-1.52E+02	-3.34E+02	3.07E+01	7.86E+01	-1.33E+02	-2.90E+00	-7.14E+00	2.23E+01	-2.51E+01	1.34E-01	2.97E-01	-1.26E+00	2.73E+00	-2.30E+00	-2.41E-03	-4.66E-03	2.54E-02	-6.92E-02	1.35E-01	-7.41E-02